# Temperature-driven spin switching and exchange bias in the $ErFeO_3$ ferrimagnet

I. Fita [1,*] R. Puzniak [1] E. E. Zubov [2] P. Iwanowski [1] and A. Wisniewski[1]

[1]*Institute of Physics, Polish Academy of Sciences, Aleja Lotnikow 32/46, PL-02668 Warsaw, Poland*

[2]*Kyiv Academic University, 36 Acad. Vernadsky Blvd., UA-03142 Kyiv, Ukraine*

(Received 30 November 2021; revised 2 February 2022; accepted 4 March 2022; published 21 March 2022)

The compensated ferrimagnet orthoferrite $ErFeO_3$ exhibits the exchange bias (EB) effect, which was previously detected as the traditional shift of the magnetization hysteresis loops $M$ vs $H$ near the compensation temperature $T_{comp} = 45$ K. This paper shows that another specific phenomenon, temperature-driven spin switching and exchange bias, occurs in this ferrimagnet. Namely, the EB manifests itself as the temperature shift of the hysteresis loops $M$ vs $T$, which occurs upon successive cooling and heating in a weak magnetic field. The $M$ vs $T$ loops limiting the region of coexistence of negative and positive magnetization are shifted towards lower or higher temperatures, depending on the sign of the applied magnetic field, which causes the unidirectional EB anisotropy. The EB anisotropy energy, which contributes to the energy barrier for switching spins to an equilibrium state, determines the shift in the switching temperature $T_{sw}$. Exchange-biased spin switching in $ErFeO_3$ is discussed within a model, which explains the magnetic compensation of the canted ferromagnetic moment of the $Fe^{3+}$ spins and the opposite moment of paramagnetic $Er^{3+}$ spins induced by the antiferromagnetic exchange interaction between the Er and Fe ions.

DOI: 10.1103/PhysRevB.105.094424

Orthoferrite $ErFeO_3$ has attracted renewed attention in recent years due to the discovery of its remarkable properties attractive for applications, such as ultrafast spin switching [1], magnetoelectric effect [2], and giant rotating magnetocaloric effect [3]. In addition, a magnon field (Dicke cooperativity) was recently discovered in $ErFeO_3$, which opens up promising prospects in quantum optics [4]. Moreover, $ErFeO_3$ is a compensated ferrimagnet [5–8] and demonstrates interesting phenomena of negative magnetization and associated fast spin switching between two coexisting states with negative and positive magnetization, which can be used to develop fast switching devices. The magnetic compensation occurs in $ErFeO_3$ because of strong antiferromagnetic (AFM) exchange interaction between $Er^{3+}$ and $Fe^{3+}$ spins, which polarizes the paramagnetic $Er^{3+}$ spins oppositely to a weak ferromagnetic (FM) moment, resulting from canted antiferromagnetic AFM ordering of Fe spins below $T_N = 636$ K due to the antisymmetric Dzyaloshinskii-Moriya (DM) exchange interaction. The paramagnetic $Er^{3+}$ moment increases with decreasing temperature while the FM moment of canted spins of $Fe^{3+}$ remains almost constant; therefore, two opposite moments cancel each other at the compensation temperature $T_{comp} = 45$ K. In an applied field, the metastable states with negative magnetization appear around $T_{comp}$, demonstrating the first-order transition at $T_{comp}$ [5]. Temperature- or field-induced spin switching to the equilibrium state with positive magnetization and minimum energy occurs when a change in the Zeeman energy upon switching overcomes the anisotropy energy barrier [9]. Similar compensated spin structures and switching between them have been identified in various orthorhombic perovskites $RMO_3$ ($R$ = rare-earth elements, $M$ = Fe, Cr, Mn) [10–16].

Recently, it was found that the spin switching in $ErFeO_3$ single crystal can be exchange biased [7]. Namely, upon cooling in an applied magnetic field, an exchange bias (EB) field arises, increases when approaching $T_{comp}$, and changes sign when crossing $T_{comp}$. The sign of EB at a given temperature can be reversed by changing the field-cooling protocol [7]. This peculiar EB in a single phase and single crystal ferrimagnetic material apparently arises due to the intrinsic exchange $4f$-$3d$ coupling within the unit cell; therefore, it is very different from traditional EB which requires an FM/AFM interface and interfacial exchange interaction between strongly anisotropic AFM and soft FM phases [17,18]. Quantum-mechanical theory was used in Ref. [19] to elucidate the EB effect and spin reversal in $ErFeO_3$. Furthermore, very similar EB behavior was later found in Nd [20], and Sm [21,22] orthoferrites around their $T_{comp}$, indicating that this striking feature is characteristic of compensated ferrimagnets. However, the complex EB behavior in $ErFeO_3$ is still not clear and its understanding requires a systematic study of spin-switching mechanism.

In this work, we show that the unidirectional anisotropy EB can manifest itself in $ErFeO_3$ not only in the traditional shift of the magnetization hysteresis loops $M$ vs $H$, but also in the temperature shift of the loops $M$ vs $T$, measured upon successive cooling and heating in a weak magnetic field. Namely, the $M$ vs $T$ loops, limiting the region of coexistence of both negative and positive magnetization, are shifted towards lower or higher temperatures, depending on the sign of the previously applied magnetic field, which causes this effect. The middle point of the $M(T)$ loop, which is generally

*ifita@ifpan.edu.pl

 

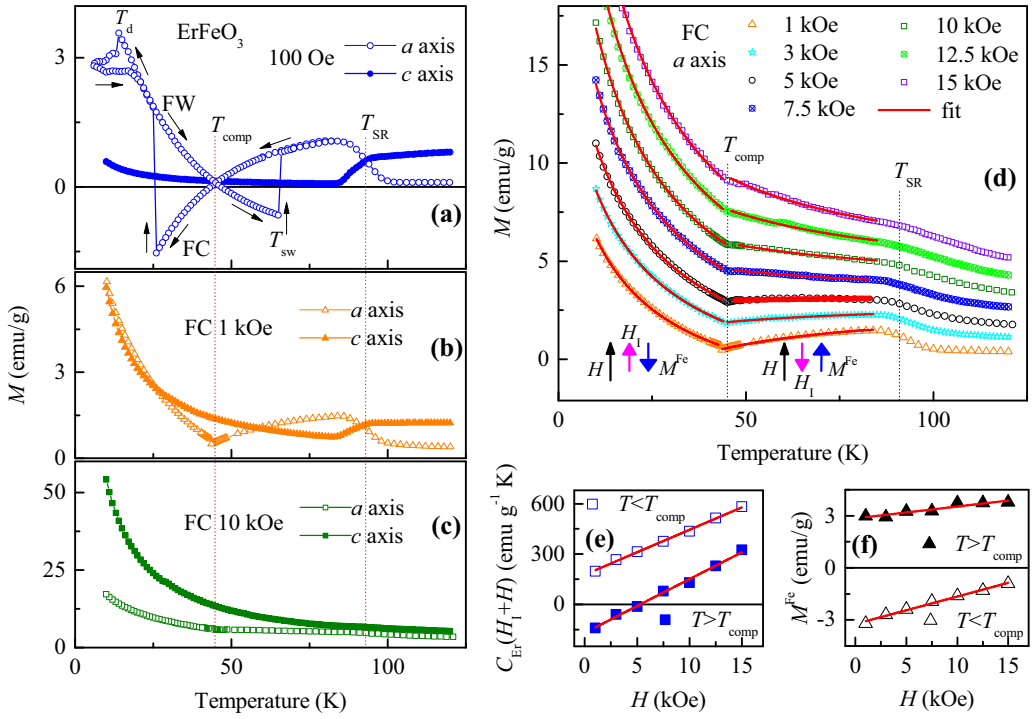


FIG. 1. Temperature dependences of the field-cooled magnetization of $ErFeO_3$ single crystal measured along both the $a$ and $c$ axes upon cooling in the fields: (a) 100 Oe, (b) 1 kOe, and (c) 10 kOe. For the $a$ axis, the $M$ vs $T$ curve obtained upon warming in a field of 100 Oe is also shown. The spin reorientation temperature $T_{SR}$, the compensation temperature $T_{comp}$, the spin-switching temperature $T_{sw}$, and the temperature $T_d$ below which the magnetic state is multidomain are indicated. (d) $M$ vs $T$ curves, taken on cooling in different magnetic fields applied along the $a$ axis. Lines in (d) represent fit with Eq. (1) with two fitting parameters, $C_{Er}(H_I + H)$ and $M^{Fe}$, shown in panels (e) and (f) as a function of field $H$. Two opposite spin configurations expected above and below $T_{comp}$ are shown in (d).

a temperature of the first-order transition at $T_{comp}$, is shifted by ~10 K from $T_{comp}$, demonstrating the EB effect. In addition, the energy required to switch the spins to an equilibrium state is comparable in the $M(T)$ and $M(H)$ loops, which confirms their common EB nature.

Magnetization measurements were performed on $ErFeO_3$ single crystals, grown by the flux method at the Weizmann Institute and previously used in magnetic studies [7,23], in the temperature range 10–250 K and in magnetic field up to 15 kOe, using a PAR (model 4500) vibrating sample magnetometer. Measurements under hydrostatic pressure up to 11 kbar were performed using a miniature CuBe container with an inner diameter of 1.4 mm [24] exploiting the silicon oil as a pressure-transmitting medium. To obtain the correct orientation of the $a$ and $c$ axes along the applied magnetic field, when the sample is mounted in the magnetometer, the crystal sample was rotated with respect to the field $H$ and the exact direction was determined using the well-known strong magnetic anisotropy of $ErFeO_3$ [3,8].

Figure 1 shows the temperature dependences of $ErFeO_3$ magnetization measured upon cooling in a magnetic field of (a) 100 Oe, (b) 1 kOe, and (c) 10 kOe applied along the $a$ and $c$ axes, as well as the curve obtained upon warming in a field of 100 Oe along the $a$ axis. The $M$ vs $T$ curve changes dramatically with an increase in the applied field $H$ due to the competing contributions of the Fe and Er magnetic sublattices. In a small field $H = 100$ Oe, a series of successive magnetic transitions is observed at the following temperatures: (1) The spin reorientation temperature $T_{SR} = 93$ K, at which the weak FM moment caused by the canted AFM ordered spins of Fe spontaneously changes its direction from the $c$ axis to the $a$ axis. (2) Compensation temperature $T_{comp} = 45$ K, at which the opposite FM moment of Fe and the moment of paramagnetic Er cancel each other and around $T_{comp}$ metastable states with negative magnetization arise due to magnetic anisotropy. (3) The spin-switching temperature $T_{sw}$, at which the magnetization suddenly changes sign from negative to positive one. (4) Finally, the temperature $T_d$ below which the single-domain magnetic state transforms into a multidomain one. The magnetization hysteresis around $T_d$ indicates the first-order transition between different magnetic states. When a stronger magnetic field is applied to the crystal, the field-induced spin reorientation transition occurs [3,8]. Namely, the total magnetic moment rotates from the $a$ axis back to the $c$ axis, which becomes the easy magnetization axis under higher field $H$ as demonstrated in Fig. 1(c). The spin reorientation in $ErFeO_3$ at $T_{SR} = 93$ K has been adequately explained in earlier work [25–27] by the competition between the magnetic anisotropy of the $Fe^{3+}$ sublattice and the single-ion anisotropy of $Er^{3+}$. The anisotropy of the $Er^{3+}$, determined by the ground multiplet $^4I_{15/2}$ ($S = 3/2$, $L = 6$), for which the easy magnetization axis is the $a$ axis, progressively increases with decreasing temperature due to an increase in the populations of the lowest Kramers doublets with energies of 0, 45, and 109 $cm^{-1}$. At a temperature of about 100 K, the anisotropy energy of $Er^{3+}$ overcomes the

weak anisotropy energy of $Fe^{3+}$ of DM origin for which the $c$ axis is the preferred magnetization axis; therefore, the FM moment rotates from the $c$ axis to the $a$ axis [25]. Similarly, the observed field-induced spin rotation back to the $c$ axis in $ErFeO_3$ can be explained by the effect of Zeeman splitting, which leads to an increase in the population in the upper Kramers doublets and, consequently, to a suppression of the $Er^{3+}$ anisotropy.

The magnetic compensation in $ErFeO_3$ can be described using a simple phenomenological model which has been well confirmed for compensated orthoferrites and orthochromites [16,20,28]. This approximation takes into account magnetization, $M^{Fe}$, arising due to the canted FM moment of Fe spins, and the opposite moment of paramagnetic $Er^{3+}$ spins induced by the AFM interaction between $Fe^{3+}$ and $Er^{3+}$ spins, so that the total magnetization in an external field $H$ is expressed as

$$M = M^{Fe} + C_{Er}(H_I + H)/(T - \theta) \quad (1)$$

Here, $C_{Er} = Ng^2\mu_B{}^2J(J+1)/3\,k_B$ is the Curie constant equal to 0.0424 emu K $g^{-1}$ $Oe^{-1}$ in the case of free $Er^{3+}$ ions for which $J = S + L = 15/2$ and $g = 6/5$, $H_I$ is the internal effective exchange field associated with induced moment of paramagnetic $Er^{3+}$ spins directed against the magnetization $M^{Fe}$, and $\theta$ is the Weiss temperature, linked to the AFM interaction between $Er^{3+}$ spins. Equation (1) was compared with the dependences of $M$ on $T$ measured in different fields $H$ applied along the $a$ axis, shown in Fig. 1(d). The curves are very different above and below $T_{comp}$ signifying that the internal $H_I$ and external $H$ fields are opposite at $T > T_{comp}$ and parallel at $T < T_{comp}$. It is clearly seen that in the temperature range between $T_{SR}$ and $T_{comp}$, the magnetization *decreases* with decreasing $T$ for $H < H_I$ and *increases* for $H > H_I$, while for $H = 5$ kOe it remains practically constant [see bold line in Fig. 1(d)]. This means that an external field of 5 kOe fully compensates the internal field in accordance with Eq. (1); therefore, $H_I \approx -5$ kOe and $M^{Fe} \approx 3$ emu/g. Solid lines in Fig. 1(d) are the best fit with Eq. (1) with two fitting parameters, $C_{Er}(H_I + H)$ and $M^{Fe}$, which vary linearly with the field $H$, as shown in Fig. 1(e) and Fig. 1(f); the constant value $\theta = -13.5$ K was maintained during the fitting. It should be noted here that the $M^{Fe}$ follows the Brillouin function $B_{S=5/2}(T)$ for the spin $S = 5/2$ of the Fe ion between $T_N = 636$ K and $T = 0$, so $M^{Fe}$ is close to the saturation value below 100 K because $B_{S=5/2}(T)$ changes only by about 1% between $T = 0$ and $T = 0.15\,T_N$. Therefore, the parameter $M^{Fe}$ in our fitting can be considered as independent of temperature. Fit shows that (i) The FM moment $M^{Fe}$ and the exchange field $H_I$ reverse their direction at temperature $T_{comp}$ and remain mutually opposite oriented. (ii) At zero field $H$, the $H_I$ field is $-5.3$ and 6.5 kOe, and the magnetization $M^{Fe}$ related with canted FM moment is equal to 2.8 and $-3.2$ emu/g, at $T > T_{comp}$ and at $T < T_{comp}$, respectively, and the modulus $M^{Fe}$ increases linearly with increasing field $H$ when it is directed along $H$ and decreases when it is directed against it. (iii) The constant $C_{Er}$ determined as the slope of the $C_{Er}(H_I + H)$ vs $H$ line in Fig. 1(e) is equal to 0.032 emu K $g^{-1}$ $Oe^{-1}$ for temperatures $T > T_{comp}$ and 0.028 emu K $g^{-1}$ $Oe^{-1}$ for $T < T_{comp}$. Almost the same value $C_{Er} = 0.031$ emu K $g^{-1}$ $Oe^{-1}$ was found for $ErFeO_3$ at 77 K in Ref. [29]. The reduced $C_{Er}$ value compared

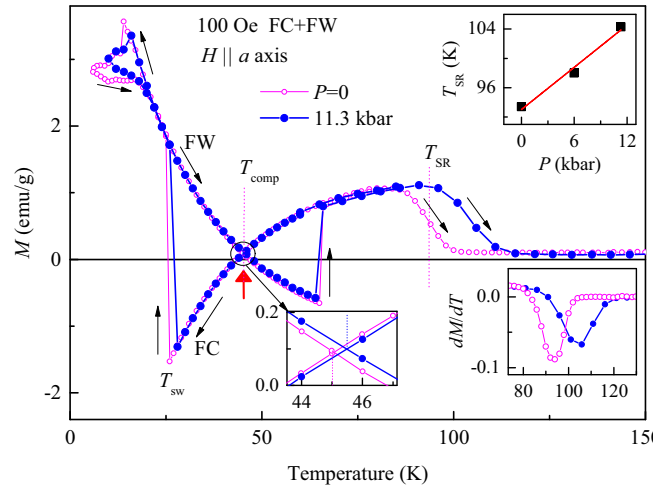


FIG. 2. Temperature dependence of $ErFeO_3$ magnetization measured in a field of 100 Oe along the $a$ axis upon cooling and then upon warming at ambient pressure $P = 0$ and at $P = 11.3$ kbar. The applied pressure leads to a significant increase in the spin reorientation temperature $T_{SR}$ (see details on the top and bottom right insets) and only slightly affects the compensation temperature $T_{comp}$ (lower left inset) and spin-switching temperatures $T_{sw}$.

to 0.0424 emu K $g^{-1}$ $Oe^{-1}$ for free $Er^{3+}$ ions is explained by a decrease in the effective magnetic moment $\mu_{eff}$ of $Er^{3+}$ with decreasing temperature due to the depopulation of the upper Kramers doublets [29]. The fact that $C_{Er}$ depends on temperature indicates that Eq. (1) does not obey exactly for $ErFeO_3$ and the obtained fitting parameters are actually averaged over the applied temperature ranges. Nevertheless, the parameters $H_I = -5.3$ kOe, $M^{Fe} = 3$ emu/g, and $\theta = -13.5$ K determined here describe well the temperature-dependent magnetization in $ErFeO_3$. For instance, the magnetization along the $a$ axis at 100 Oe and $T = 80$ K, calculated with Eq. (1), $M_{calc} = 1.15$ emu/g, is close to the experimental value of 1.1 emu/g, see Fig. 1(a) and Refs. [3,8]. In addition, the compensation temperature $T_{comp}{}^{calc} = 43$ K, calculated by the formula $T_{comp} = (C_{Er}H_I/M^{Fe}) + \theta$, which follows from Eq. (1) at $M = 0$ and $H = 0$, also agrees well with the observed $T_{comp} = 45$ K.

Pressure is an effective tool for adjusting the magnetic properties of perovskite oxides. Figure 2 shows the effect of a hydrostatic pressure of 11.3 kbar on the $M$ vs $T$ curves of $ErFeO_3$ measured in a field of 100 Oe along the $a$ axis upon cooling (FC) and then upon warming (FW). Interestingly, the applied pressure leads to a significant increase in the spin reorientation temperature $T_{SR}$ and only slightly affects the magnetization at lower temperatures. Temperature $T_{SR}$, defined as the temperature of the minimum in derivative $dM/dT$ (see bottom inset), increases under pressure with a coefficient $dT_{SR}/dP = 0.96$ K/kbar (see upper inset), which is in qualitative agreement with the previously reported behavior [30]. In contrast, the compensation temperature $T_{comp}$, defined as the temperature of crossing the FC and FW magnetization branches, increases at a pressure of 11.3 kbar by only about 0.5 K (see left lower inset), and also the spin-switching temperatures $T_{sw}$ change insignificantly. According to the above

formula for $T_{comp}$, this indicates that the $C_{Er}H_I/M^{Fe}$ ratio changes slightly in $ErFeO_3$ under pressure, i.e., the balance of two opposite magnetic moments is maintained. There are no data in the literature concerning the dependence of the parameters $H_I$ and $M^{Fe}$ on the pressure in orthoferrites, but there is a prediction based on first-principles calculations that the canted FM moment $M^{Fe}$ in $SmFeO_3$ should increase by about 1.4% at a pressure of 10 kbar [31]. Therefore, it can be expected that the internal field $H_I$ and the associated Er-Fe exchange interaction will also change in order. Such small changes in the Er-Fe interaction cannot be the reason for the observed strong increase in temperature $T_{SR}$ under pressure. Note here that anisotropic interactions between $R$ and Fe ions were suggested to be responsible for the spin reorientation in orthoferrites [32]. In the framework of the alternative scenario discussed above, according to which the SR transition occurs when the anisotropy energy of $Er^{3+}$ overcomes the weak anisotropy energy of $Fe^{3+}$ of DM origin [25–27], it can be assumed that the applied pressure leads to an increase in the crystal-field splitting of the multiplet $Er^{3+}$. If this is the case, then the energy distance between the lowest Kramers doublets increases; therefore, the redistribution in their population and, accordingly, the spin reorientation, occurs under pressure at higher temperatures. However, to test this plausible scenario, it is necessary to investigate the $Er^{3+}$ energy levels in $ErFeO_3$ under pressure using optical spectroscopy.

The fact that the switching temperature $T_{sw}$ changes insignificantly at a pressure of 11.3 kbar means that the energy barrier for switching between the two opposite spin configurations shown in Fig. 1(d) weakly depends on pressure. The energy barrier here is the energy of magnetic anisotropy of the crystal which provides the phenomenon of negative magnetization in compensated ferrimagnets [9]. In the absence of magnetic anisotropy, there is no negative magnetization and therefore no spontaneous spin switching (magnetization reversal), since the net magnetization is always directed along the applied field $H$, above and below $T_{comp}$. In the case of nonzero anisotropy, negative magnetization and hysteresis of the FC and FW magnetization branches centered at $T_{comp}$ appear in the $M$ vs $T$ loop (in the form of a butterfly), which is a characteristic of the first-order magnetic transition at $T_{comp}$, see Fig. 2. When a stronger field $H$ is applied, the magnetic anisotropy is suppressed, so the negative magnetization disappears, the hysteresis decreases, and both temperatures $T_{sw}$ approach $T_{comp}$, as seen in Fig. 1. The fall in the Zeeman energy $\Delta E_Z = -\Delta MH$ upon spin switching with a change in the magnetization $\Delta M$ at $T_{sw}$ is a measure of the energy barrier that the system must overcome in order to pass from a metastable state to a thermodynamically equilibrium state. In what follows, we will show that the energy barrier and therefore the switching temperature $T_{sw}$ can be controlled by a magnetic field $H$ applied under certain conditions. Figure 3 shows several $M$ vs $T$ loops of $ErFeO_3$, measured in the same low field of 50 Oe along the $a$ axis upon cooling and subsequent warming but taken under different conditions. Namely, before each measurement at $H = 50$ Oe, the field $H^*$ equal to $+10$ kOe or $-10$ kOe (polarity relative to measurement field $H$) was applied for a short time of 5 min at temperatures much higher than $T_{comp}$ ($T = 85$ K) and much lower than $T_{comp}$ ($T = 10$ K). This manipulation has a remarkable effect: the

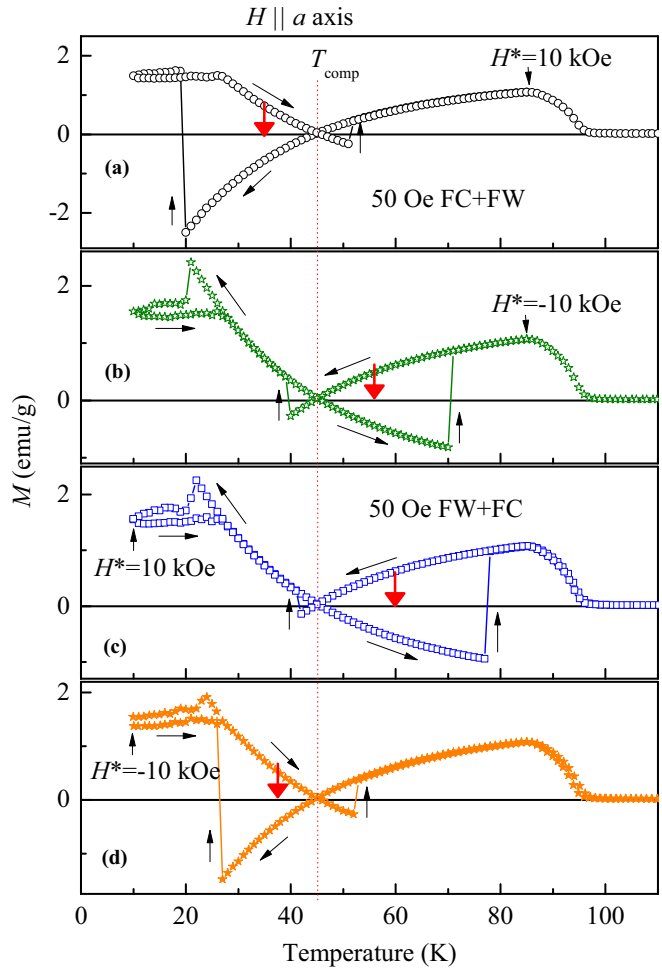


FIG. 3. Temperature dependences of $ErFeO_3$ magnetization measured in a field of 50 Oe along the $a$ axis under conditions: (a), (b) upon cooling and subsequent warming after a short-term application of the field $H^* = \pm 10$ kOe at $T = 85$ K; (c), (d) upon warming and then cooling after a short-term application of the field $H^* = \pm 10$ kOe at $T = 10$ K. The hysteresis loop, which limits the region of coexistence of both negative and positive magnetization, shifts towards lower or higher temperatures depending on the sign of the field $H^*$. The middle point of the loop (indicated by the bold red arrow) is displaced by about 10 K from $T_{comp}$, demonstrating the exchange bias effect.

loop $M$ vs $T$, exposed to positive $H^*$ at 85 K, shifts towards lower temperatures, and the loop after exposure to negative $H^*$ shifts to higher $T$, see Figs. 3(a) and 3(b). In particular, the midpoint of the hysteresis loops $M$ vs $T$ is displaced by about 10 K from $T_{comp}$ (compare with the loop in Fig. 2 which is not affected by $H^*$, so it is unbiased and its center is $T_{comp}$). On the other hand, the FC magnetizations in both loops coincide at $T > T_{comp}$, and the FW magnetizations also coincide below $T_{comp}$, and $T_{comp}$ is the same. It appears that the effect of the field $H^*$ leads only to a change in the temperatures $T_{sw}$ and, hence, to a change of the energy barriers for spin switching. In the case of a positive $H^*$, the left-hand $T_{sw}$ moves away from $T_{comp}$ and the magnetization jump $\Delta M$ at $T_{sw}$ becomes huge, while the right-hand $T_{sw}$ approaches $T_{comp}$ and $\Delta M$ decreases, see Fig. 3(a). Consequently, the energy barrier, estimated as a

fall in the Zeeman energy $\Delta E_Z = -\Delta MH$ at $T_{sw}$, for the spin switching which occurs below $T_{comp}$ becomes several times larger than the barrier for the reverse spin switching, which occurs above $T_{comp}$. When a negative field $H^* = -10$ kOe is applied at $T = 85$ K, the picture is exactly the opposite: now the energy barrier for reverse spin switching is much higher than for spin switching below $T_{comp}$. This striking behavior clearly indicates that the field $H^*$ induces the unidirectional anisotropy (EB anisotropy) along the $a$ axis, which forms an energy barrier for spin switching, and the sign of EB is determined by whether the field $H^*$ and the total magnetization $M$ are parallel or opposite. In addition, if the field $H^*$ is applied at a low temperature of 10 K, at which the FM moment of Fe and the moment of paramagnetic Er are opposite to their directions at $T > T_{comp}$, the effect is similar to that described above, but has the opposite sign [see Figs. 3(c) and 3(d)].

We compare the EB effect pronounced well in the $M$ vs $T$ hysteresis loops with the EB that has been found in $ErFeO_3$ in the vicinity of $T_{comp}$, derived from the $M$ vs $H$ hysteresis loops in Ref. [7]. Figure 4 shows several hysteresis loops $M$ vs $H$ for $ErFeO_3$, recorded in fields between 10 kOe and −10 kOe applied along the $a$ axis at a temperature of 50 K after various FC procedures. They evidence a negative EB field $H_{EB} \approx -500$ Oe for the case when a FC field of 10 kOe is applied at 300 K, and a positive $H_{EB} \approx 500$ Oe when the FC field is −10 kOe. Here, $H_{EB}$ (marked by a bold red arrow) is defined as $H_{EB} = (H_1 + H_2)/2$ and the switching fields $H_1$ and $H_2$ are true coercive fields [see Figs. 4(a) and 4(b)]. Moreover, when the FC with 10 kOe was completed from 300 K to temperature $T^* = 10$ K and then $M$ vs $H$ loop was measured at 50 K, the field $H_{EB}$ was also positive and close to 500 Oe, as shown in Fig. 4(c). Interestingly, there is an exact analogy in the field-induced change in the hysteresis loops $M$ vs $H$ and $M$ vs $T$ presented in Figs. 4(a), 4(b), 4(c) and Figs. 3(a), 3(b), 3(c), respectively. This is convincing evidence of the same field-induced EB effect, which manifests itself in both types of hysteresis loops. The energy associated with EB anisotropy, calculated as the difference between the changes in Zeeman energy $\Delta E_Z = -\Delta MH$ in the two spin switching field $H_1$ and $H_2$ in the loop $M$ vs $H$ [Fig. 4(a)], or in the case of a loop $M$ vs $T$ at two switching temperatures $T_{sw}$ [Fig. 4(a)], are comparable in magnitude: ≈ 300 and ≈ 170 emu Oe/g, respectively. If one considers that the field-induced energy of the $-\Delta MH$ form determines the EB effect, it is understandable why the EB effect is well detected with the $M$ vs $H$ loops solely in the vicinity $T_{comp}$ when $\Delta M$ is small enough [7]. On the contrary, the effect is clearly seen in the $M$ vs $T$ loops when $H$ is small and $\Delta M$ is huge. In addition, the EB effect in $ErFeO_3$ at given temperature can be controlled by adjusting the FC process. Figure 4 shows that the loop $M$ vs $H$ completed between ±10 kOe at 50 K evolves, and the field $H_{EB}$ at 50 K changes sign and can also take a zero value [see inset in Fig. 4(f)] when the sample was differently cooled in a magnetic field prior to loop measurement. Specifically, the sample was cooled in a field of 10 kOe from 300 K to various temperatures $T^* = 10$, 20, 30, 40, 50 K and then heated in the same field to $T = 50$ K. Thus, an interesting property of $ErFeO_3$ can be distinguished: different signs and values of EB can be realized at each given temperature, depending on the complexity of the field cooling/heating process.

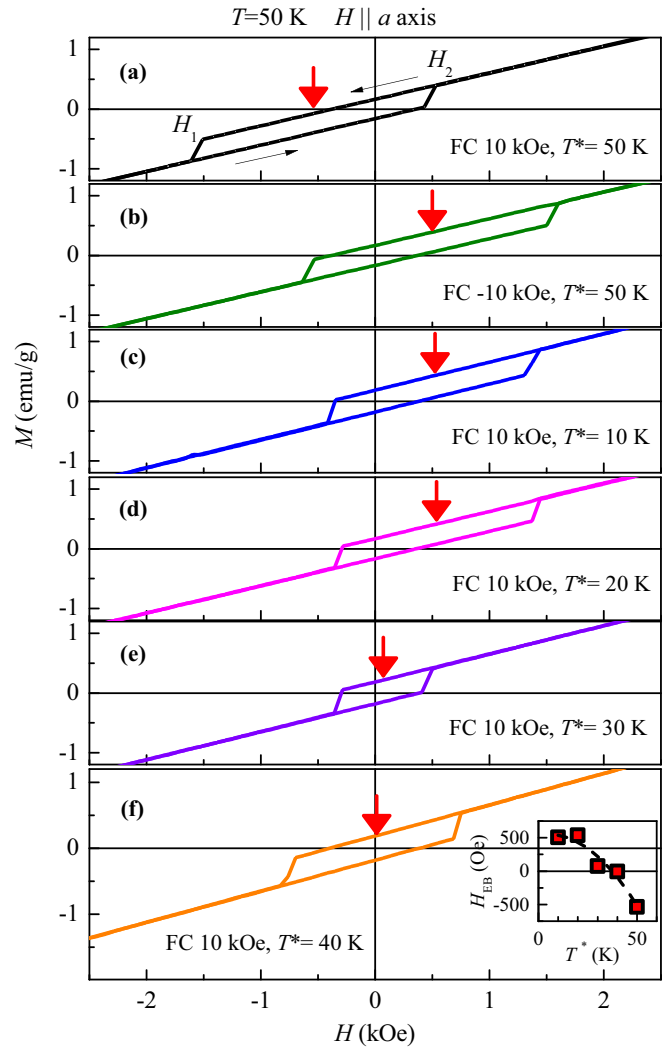


FIG. 4. Magnetization hysteresis loops of $ErFeO_3$, in an extended scale, recorded between 10 and −10 kOe fields along the $a$ axis at temperature $T = 50$ K after various field-cooling procedures: (a), (b) FC in ±10 kOe to 50 K; (c), (d), (e), (f) FC in 10 kOe to the temperature $T^* = 10$ K (c), 20 K (d), 30 K (e), 40 K (f), and subsequent warming in same field up to $T = 50$ K. The exchange bias field $H_{EB}$ (midpoint of the loop marked with an arrow) changes its value and sign as $T^*$ increases from 10 to 50 K, as shown in the inset to panel (f).

Figure 5(a) shows the $M$ vs $T$ curves of $ErFeO_3$ measured in a field of 50 Oe along the $a$ axis upon warming after a short exposure in different fields $H^*$ up to ±15 kOe at $T = 10$ K. They indicate that the spin-switching temperature $T_{sw}$ is either about 50 or about 75 K, due to the EB effect induced by the field $H^*$, while the magnetization in modulus does not depend on $H^*$, and $T_{comp}$ also does not change within 0.1%. Among them, the curve obtained with a low value of $H^* = 50$ Oe is not exchange-biased and shows an average temperature $T_{sw} = 64$ K. It appears that just a moderate field $H^*$ of about ±1 kOe is required to induce an EB and, therefore, shift $T_{sw}$ to values of 50 or 75 K [see inset in Fig. 5(a)]. It should be noted that a qualitatively similar dependence of $T_{sw}$ on $H^*$, in fields an order of magnitude higher only, was also observed

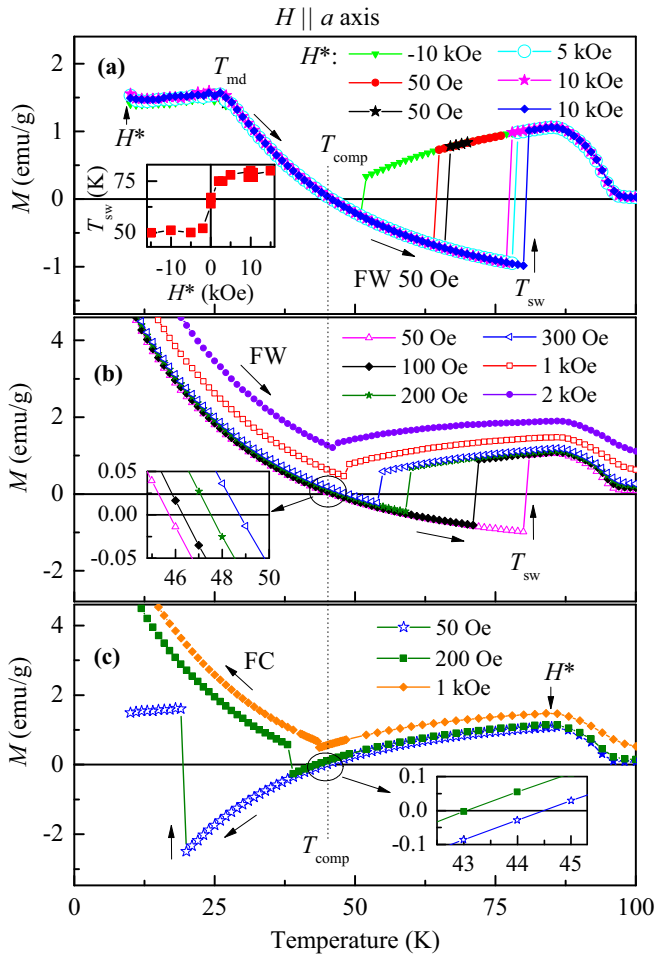


FIG. 5. Temperature dependences of $ErFeO_3$ magnetization measured along the *a* axis under conditions: (a) in a field of 50 Oe upon warming after a short exposure in a field of different values of $H^*$ at $T = 10$ K. The inset shows the dependence of the spin-switching temperature $T_{sw}$ on $H^*$; (b), (c) in different measuring fields $H$ (b) upon warming after exposure to a field $H^* = 10$ kOe at $T = 10$ K and (c) upon cooling after exposure to a field $H^* = 10$ kOe at $T = 85$ K. The temperature $T_{comp}$, at which the magnetization $M$ vanishes, increases in warming mode (b) and decreases in cooling mode (c) with increasing field $H$, as shown in the insets.

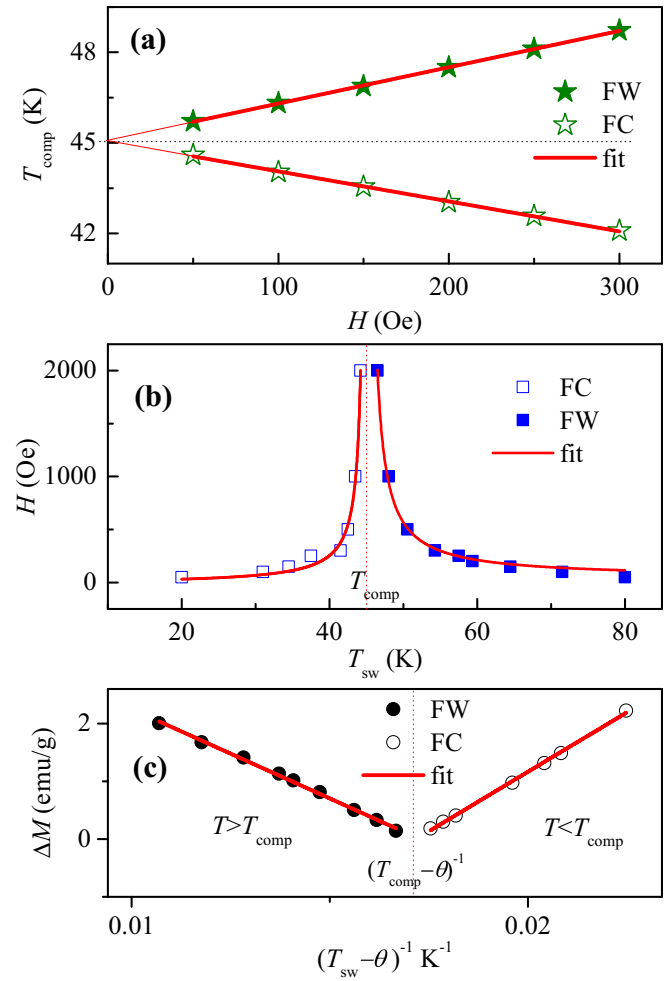


FIG. 6. (a) Linear increase/decrease in the compensation temperature $T_{comp}$ with increasing field $H$ in the cases of FW/FC magnetization modes. (b) The dependences of the spin-switching temperature $T_{sw}$ on the field $H$ below and above $T_{comp}$. The lines represent the best fit with Eq. (2) for two parameters, $\Delta E_Z/2M^{Fe}$ and $T_{comp}$. (c) The jump in magnetization $\Delta M$ at $T_{sw}$, taken as a function of $(T_{sw} - \theta)^{-1}$ below and above $T_{comp}$, and the lines present linear approximation.

in $SmFeO_3$ (see Fig. 2 in Ref. [22]), which suggests that such behavior is characteristic of compensated ferrimagnets. Next, the dependence of the switching temperature $T_{sw}$ on the measuring field $H$ was investigated at a constant field $H^*$. The field $H^* = 10$ kOe was applied for a short time at $T = 10$ K [see the $M$ vs $T$ curves in the FW mode in Fig. 5(b)] and at $T = 85$ K [see the $M$ vs $T$ curves in the FC mode in Fig. 5(c)]. In both cases, the temperature $T_{sw}$ approaches $T_{comp}$ with increasing $H$, and at the same time the jump in the magnetization $\Delta M$ at $T_{sw}$ decreases. In contrast, the compensation temperature $T_{comp}(H)$, at which the FW magnetization vanishes for a given $H$, at which negative $M$ still exists, increases [see inset in Fig. 5(b)], while in the case of FC magnetization this temperature decreases [see inset in Fig. 5(c)]. Figure 6(a) shows a linear increase/decrease in $T_{comp}(H)$ with $H$ for the cases of FW/FC magnetization modes, respectively, and the linear approximations show the same $T_{comp}(H = 0) = 45.1$ K and different slopes of $1.20 \times 10^{-2}$ K/Oe in FW mode and $-0.99 \times 10^{-2}$ K/Oe in FC mode. Comparing these results with the formula $T_{comp}(H) = (C_{Er}(H_I + H)/M^{Fe}) + \theta$, which follows from Eq. (1) at $M = 0$, where $\theta = -13.5$ K, we calculate the values of the effective exchange field $H_I = -4.9$ kOe at $T > T_{comp}$ and 5.9 kOe at $T < T_{comp}$. The obtained values are in good agreement with those obtained from the analysis of magnetization shown in Fig. 1(d), thus repeating once again that the exchange field $H_I$ is greater in magnitude by about 20% at $T < T_{comp}$, in the magnetic phase with a predominant magnetic moment Er directed along the field $H$.

Figure 6(b) shows that both switching temperature $T_{sw}$, which occur above and below $T_{comp}$, approach $T_{comp}$ with increasing field $H$. The $H_{sw}$-$T_{sw}$ lines represent the boundaries between magnetic phases with two opposite spin configurations, between which fast switching occurs. On the $H$-$T$

diagram, the region of metastable states is located between the $H_{sw}$-$T_{sw}$ lines, and the equilibrium magnetic states are above them. It should be noted that both lines are exchange-biased but in different ways; they are shifted in temperature from $T_{comp}$ due to the exchange bias effect caused by the action of a field $H^* = 10$ kOe at temperatures 10 or 85 K. The $H_{sw}$-$T_{sw}$ lines were examined within the model represented by Eq. (1). According to Eq. (1), the fall in the Zeeman energy at spin switching is equal to $\Delta E_Z = \Delta MH = 2[M^{Fe} - C_{Er}H_I/(T_{sw} - \theta)]H$, and taking into account that $T_{comp} = (C_{Er}H_I/M^{Fe}) + \theta$, the switching field $H_{sw}$ as a function of temperature can be expressed as follows:

$$H_{sw} = -\left(\Delta E_Z/2M^{Fe}\right)(T - \theta)/(T - T_{comp}) \qquad (2)$$

Solid lines in Fig. 6(b) at temperatures above and below $T_{comp}$ represent the best fit with Eq. (2) for the values of two fitting parameters $\Delta E_Z/2M^{Fe} = -23$ and 43 Oe and $T_{comp} = 44.8$ and 45.2 K, respectively, at a constant value $\theta = -13.5$ K. Taking into account the magnetization of canted FM moment $M^{Fe} = 2.8$ and $-3.3$ emu/g, determined above and below $T_{comp}$, we estimate the corresponding switching energies $\Delta E_Z = 150$ and 240 emuOe/g, which determine the lines in the $H$-$T$ plane, at which a spontaneous spin reversal occurs. We recall that the obtained $\Delta E_Z$ energies contain different contributions EB, since for each line the EB effect was induced differently, as described above.

The jump in magnetization $\Delta M$ at $T_{sw}$, which is associated with the energy barrier for spin switching, decreases rapidly with increasing applied field $H$ as $T_{sw}$ approaches $T_{comp}$, see Figs. 5(b) and 5(c). In fact, this behavior reflects the vanishing magnetization $M$ as $T$ approaches $T_{comp}$, since $\Delta M = 2M$ when the magnetization reverses direction. According to Eq. (1), the change in magnetization at $T_{sw}$ which occurs above $T_{comp}$ is $\Delta M = 2M^{Fe} - 2C_{Er}H_I/(T_{sw} - \theta)$, and $\Delta M = -2M^{Fe} + 2C_{Er}H_I/(T_{sw} - \theta)$ when the spin switching occurs below $T_{comp}$. In Fig. 6(c) the jump in magnetization $\Delta M$, measured at each temperature $T_{sw}$ shown in Fig. 6(b), is taken as a function of $(T_{sw} - \theta)^{-1}$, and the lines represent linear approximation. It appears that Eq. (1) describes well the sharp change in magnetization at the switching temperature $T_{sw}$ and predicts the magnetization of canted FM moment $M^{Fe} = 2.67$ emu/g at temperatures above $T_{comp}$ and $-3.5$ emu/g below $T_{comp}$. In addition, keeping constant $C_{Er} = 0.032$ emu K g$^{-1}$ Oe$^{-1}$, we estimate from the line slopes the exchange field $H_I = -4.8$ kOe for $T > T_{comp}$ and 6.4 kOe for $T < T_{comp}$. Thus, successive fittings of Eq. (1) performed for various $ErFeO_3$ characteristics, such as compensation temperature $T_{comp}$, spin-switching temperature $T_{sw}$, and magnetization jump at $T_{sw}$, show good agreement with practically the same $H_I$ and $M^{Fe}$ parameters for each of the temperature ranges above and below $T_{comp}$. However, it turns out that the parameters above $T_{comp}$ differ from those below $T_{comp}$; namely, the values of both $H_I$ and $M^{Fe}$ in the phase with a predominant magnetic moment Er are approximately 25% larger than in the phase with a predominant FM moment of canted spins of Fe. Further study is required to understand this cryptic behavior.

Let us briefly summarize the scenario of the EB effect, which can manifest itself simultaneously in both hysteresis loops $M$ vs $H$ and $M$ vs $T$ in the compensated ferrimagnet

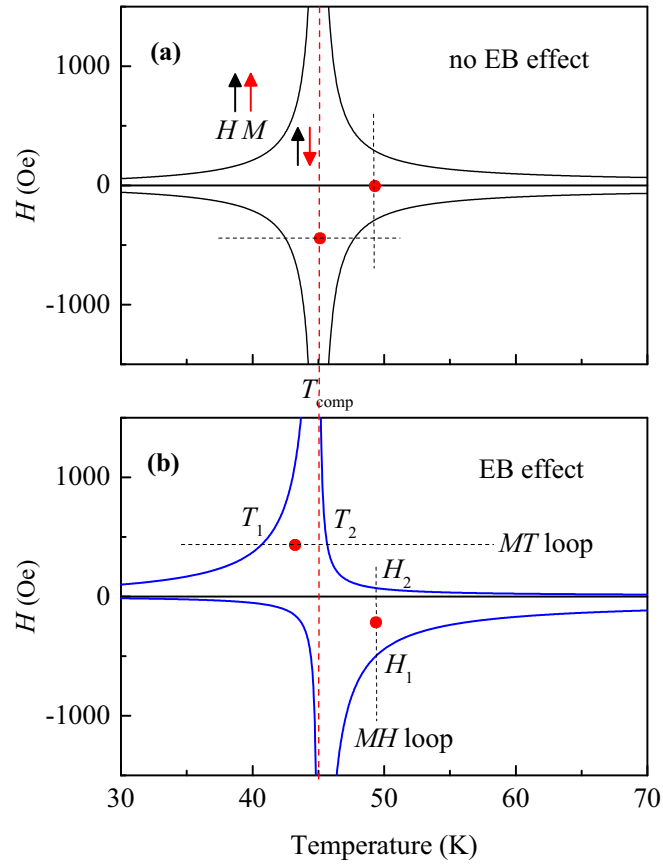


FIG. 7. Spin-switching lines in the $H$-$T$ plane, calculated using Eq. (2) for the cases of absence (a) and presence (b) of unidirectional EB anisotropy (see the text for details). The asteroidlike lines $H_{sw}$-$T_{sw}$, limiting the region of metastable magnetic states (negative magnetization), turn out to be almost symmetric with respect to both axes $T = T_{comp}$ and $H = 0$ in the case of conventional uniaxial magnetic anisotropy (a), but with the introduction of unidirectional anisotropy they become asymmetric (b), providing a shift in the center of both $M$ vs $H$ and $M$ vs $T$ hysteresis loops (EB effect).

$ErFeO_3$, based on a compensation model that gives a relationship between the field and the spin-switching temperature [see Eq. (2)]. Recall that switching between the two opposite spin configurations, namely, from a metastable state with the negative magnetization to a thermodynamically equilibrium state, is determined by an energy barrier which is the energy of the magnetic anisotropy of the crystal. In the absence of magnetic anisotropy, spontaneous spin switching (magnetization reversal) does not occur. Below, we demonstrate that the character of spin switching depends on the type of magnetic anisotropy. Figure 7(a) shows the spin-switching lines obtained from Eq. (2) by taking into account only uniaxial magnetic anisotropy $K$, which means the same energy barrier for spin-up and -down switching. Namely, all $H_{sw}$-$T_{sw}$ lines are calculated for $\Delta E_Z = K$ at the same conditional value $K/2M^{Fe} = 20$ Oe and at $T_{comp} = 45$ K, $\theta = -13.5$ K. These asteroidlike lines restrict the region of metastable states, which collapses at the point $T = T_{comp}$, $H = 0$ when the anisotropy $K$ decreases to zero. It is important that, due to the property of uniaxial anisotropy, the $H_{sw}$-$T_{sw}$ lines are almost

symmetric with respect to both axes $T = T_{comp}$ and $H = 0$, which leads to the symmetry of the hysteresis loops of both $M$ vs $H$ and $M$ vs $T$, i.e., EB effect is absent. This picture changes radically when the unidirectional anisotropy $U$ is added to the uniaxial anisotropy $K$, induced by the magnetic field $H^*$ applied far from $T_{comp}$. The unidirectional anisotropy $U$ acts in such a way that the energy barrier for spin switching in one direction of the easy axis increases to a value of $K + U$, and in the opposite direction decreases to $K - U$. Figure 7(b) shows the $H_{sw}$-$T_{sw}$ lines calculated from Eq. (2), taking different values $\Delta E_Z = K \pm U$ for opposite spin directions with conditional values $K/2M^{Fe} = 20$ Oe and $U/2M^{Fe} = 15$ Oe, and at $T_{comp} = 45$ K, $\theta = -13.5$ K. It turns out that the unidirectional anisotropy $U$, introducing the nonequivalence of spin directions along the easy axis, makes the $H_{sw}$-$T_{sw}$ lines substantially asymmetric with respect to the axes $T = T_{comp}$ and $H = 0$. This results in a shift in the center of both $M$ vs $H$ and $M$ vs $T$ hysteresis loops, as shown in Fig. 7(b), by the value of $H_{EB} = (H_1 + H_2)/2$ from the axis $H = 0$, and by value of $\Delta T_{EB} = (T_1 + T_2)/2 - T_{comp}$ from the axis $T = T_{comp}$, respectively. Both parameters $H_{EB}$ and $\Delta T_{EB}$ equally characterize the EB effect in compensated ferrimagnet: $H_{EB}$ increases rapidly as the temperature approaches $T_{comp}$, which was observed in the experiment, and $\Delta T_{EB}$ similarly increases speedily as the magnetic field $H$ decreases. The signs of the shifts $H_{EB}$ and $\Delta T_{EB}$ depend on the direction resulting from unidirectional anisotropy created by the field $H^*$. The diagram in Fig. 7(b), calculated for the case of the direction resulting from $U$ changes, providing a higher energy barrier for spin switching at $T < T_{comp}$ and $H > 0$, shows a negative $H_{EB}$ for $T > T_{comp}$, as well as negative $\Delta T_{EB}$ for $H > 0$. The same sign in $H_{EB} \approx -500$ Oe and $\Delta T_{EB} \approx -10$ K is observed in the case of a positive $H^* = 10$ kOe applied well above $T_{comp}$ [see Fig. 4(a) and Fig. 3(a)]. Conversely, when the direction resulting from $U$ changes is reversed by setting a higher energy barrier to switch the spin at $T > T_{comp}$, the pattern of the $H_{sw}$-$T_{sw}$ lines becomes mirrored with respect to Fig. 7(b) (not shown), while the sign in $H_{EB}$ and $\Delta T_{EB}$ changes. This is exactly what we observe experimentally, when the unidirectional EB anisotropy changes sign upon application of a negative field $H^* = -10$ kOe, namely, $H_{EB} \approx +500$ Oe and $\Delta T_{EB} \approx +10$ K [Fig. 4(b) and Fig. 3(b)]. In addition, the ensemble of asymmetric $H_{sw}$-$T_{sw}$ lines in Fig. 7(b) qualitatively resembles the temperature behavior of the switching fields $H_1$ and $H_2$ obtained for the FC regime both for $ErFeO_3$ (see Fig. 4(b) in Ref. [7]) and for a similar compensated ferrimagnet $GdCrO_3$ at $T > T_{comp}$ (see Fig. 4(a) in Ref. [16]). On the contrary, the exactly symmetrical $H_{sw}$-$T_{sw}$ lines observed in $GdCrO_3$ at temperatures below $T_{comp}$ (due to the absence of the EB effect) resemble the calculated lines for the case of the absence of unidirectional anisotropy $U$ in Fig. 7(a). Thus, the intuitive compensation model used well reproduces the main features of the $M$ vs $H$ and $M$ vs $T$ hysteresis loops due to the EB effect in the compensated $ErFeO_3$ and $GdCrO_3$ ferrimagnets.

In conclusion, the exchange bias in $ErFeO_3$ is clearly manifested not only in the traditional field shift $H_{EB}$ of the $M$ vs $H$ hysteresis loops near $T_{comp}$, but also in the temperature shift $\Delta T_{EB}$ of the $M$ vs $T$ hysteresis loops, completed upon successive cooling and heating in a weak magnetic field. Both parameters $H_{EB} = (H_1 + H_2)/2$ and $\Delta T_{EB} = (T_1 + T_2)/2 - T_{comp}$ equally characterize the EB effect in a compensated ferrimagnet. This is because both the spin-switching field $H_{sw}$ and the switching temperature $T_{sw}$ are equally dependent on the energy barrier containing the contribution of the unidirectional anisotropy EB as soon as the EB is induced by an applied magnetic field in temperatures far from $T_{comp}$. The energy required to switch the spins to equilibrium appears to be comparable in the $M$ vs $T$ and $M$ vs $H$ loops, which confirms their common EB nature. The switching energy in the $-\Delta MH$ form explains why the EB effect is well detected with $M$ vs $H$ loops mainly near $T_{comp}$, when the magnetization jump $\Delta M$ is small, and conversely, the effect is clearly seen in the $M$ vs $T$ loops when $H$ is small and $\Delta M$ is huge.

The authors are grateful to Prof. G. Gorodetsky and Dr. V. Markovich for providing high-quality $ErFeO_3$ crystals.

[1] J. A. de Jong, A. V. Kimel, R. V. Pisarev, A. Kirilyuk, and Th. Rasing, Phys. Rev. B **84**, 104421 (2011).
[2] D. G. Oh, J. H. Kim, H. J. Shin, and Y. J. C. N. Lee, Sci. Rep. **10**, 11825 (2020).
[3] R. Huang, S. Cao, W. Ren, S. Zhan, B. Kang, and J. Zhang, Appl. Phys. Lett. **103**, 162412 (2013).
[4] X. Li, M. Bamba, N. Yuan, Q. Zhang, Y. Zhao, M. Xiang, K. Xu, Z. Jin, W. Ren, G. Ma, S. Cao, D. Turchinovich, and J. Kono, Science **361**, 794 (2018).
[5] V. N. Derkachenko, A. M. Kadomtseva, V. A. Timofeeva, and V. A. Khokhlov, JETP Lett. **20**, 104 (1974).
[6] L. T. Tsymbal, Ya. B. Bazaliy, V. N. Derkachenko, V. I. Kamenev, G. N. Kakazei, F. J. Palomares, and P. E. Wigen, J. Appl. Phys. **101**, 123919 (2007).
[7] I. Fita, A. Wisniewski, R. Puzniak, V. Markovich, and G. Gorodetsky, Phys. Rev. B **93**, 184432 (2016).
[8] X. X. Zhang, Z. C. Xia, Y. J. Ke, X. Q. Zhang, Z. H. Cheng, Z. W. Ouyang, J. F. Wang, S. Huang, F. Yang, Y. J. Song, G. L. Xiao, H. Deng, and D. Q. Jiang, Phys. Rev. B **100**, 054418 (2019).
[9] A. Kumar and S. M. Yusuf, Phys. Rep. **556**, 1 (2015).
[10] J.-H. Lee, Y. K. Jeong, J. H. Park, M.-A. Oak, H. M. Jang, J. Y. Son, and J. F. Scott, Phys. Rev. Lett. **107**, 117201 (2011).
[11] J.-S. Jung, A. Iyama, H. Nakamura, M. Mizumaki, N. Kawamura, Y. Wakabayashi, and T. Kimura, Phys. Rev. B **82**, 212403 (2010).
[12] S. Yuan, W. Ren, F. Hong, Y. B. Wang, J. C. Zhang, L. Bellaiche, S. X. Cao, and G. Cao, Phys. Rev. B **87**, 184405 (2013).
[13] S. Cao, H. Zhao, B. Kang, J. Zhang, and W. Ren, Sci. Rep. **4**, 5960 (2014).

[14] Y. Sun, J.-Z. Cong, Y.-S. Chai, L.-Q. Yan, Y.-L. Zhao, S.-G. Wang, W. Ning, and Y.-H. Zhang, Appl. Phys. Lett. **102**, 172406 (2013).
[15] Y. Cao, S. Cao, W. Ren, Z. Feng, S. Yuan, B. Kang, B. Lu, and J. Zhang, Appl. Phys. Lett. **104**, 232405 (2014).
[16] I. Fita, R. Puzniak, A. Wisniewski, and V. Markovich, Phys. Rev. B **100**, 144426 (2019); I. Fita, R. Puzniak, and A. Wisniewski, *ibid.* **103**, 054423 (2021).
[17] W. H. Meiklejohn and C. P. Bean, Phys. Rev. **102**, 1413 (1956).
[18] J. Nogués, J. Sort, V. Langlais, V. Skumryev, S. Suriñach, J. S. Muñoz, and M. D. Baró, Phys. Rep. **422**, 65 (2005).
[19] E. E. Zubov, V. Markovich, I. Fita, A. Wisniewski, and R. Puzniak, Phys. Rev. B **99**, 184419 (2019).
[20] I. Fita, A. Wisniewski, R. Puzniak, E. E. Zubov, V. Markovich, and G. Gorodetsky, Phys. Rev. B **98**, 094421 (2018).
[21] X. Wang, S. Gao, X. Yan, Q. Li, J. Zhang, Y. Long, K. Ruan, and X. Li, Phys. Chem. Chem. Phys. **20**, 3687 (2018).
[22] S. L. Ding, M. Z. Xue, Z. Y. Liang, Z. Liu, R. B. Li, S. X. Cao, Y. B. Sun, J. J. Zhao, W. Y. Yang, and J. B. Yang, J. Phys.: Condens. Matter. **31**, 435801 (2019).
[23] G. Gorodetsky, and B. Lüthi, Phys. Rev. B **2**, 3688 (1970); G. Gorodetsky, L. M. Levinson, S. Shtrikman, D. Treves, and B. M. Wanklyn, Phys. Rev. **187**, 637 (1969).
[24] M. Baran, V. Dyakonov, L. Gladczuk, G. Levchenko, S. Piechota, and H. Szymczak, Physica C **241**, 383 (1995).
[25] D. L. Wood, J. P. Remeika, L. M. Holmes, and E. M. Gyorgy, J. Appl. Phys. **40**, 1245 (1969).
[26] R. L. White, J. Appl. Phys. **40**, 1061 (1969).
[27] A. I. Belyaeva and K. V. Baranova, Izv. Ross. Akad. Nauk, Ser. Fiz. **73**, 1117 (2009) [Bull. Russ. Acad. Sci.: Phys. **73**, 1056 (2009)].
[28] A. H. Cooke, D. M. Martin, and M. R. Wells, J. Phys. C: Solid State Phys. **7**, 3133 (1974).
[29] I. Mikami, J. Phys. Soc. Jpn. **34**, 338 (1973).
[30] G. H. Hu, I. Umehara, X. Shuang, S. Yuan, and S. X. Cao, J. Phys.: Conf. Ser. **400**, 032023 (2012).
[31] H. J. Zhao, W. Ren, y. Yang, X. M. Chen, and L. Bellaiche, J. Phys.: Condens. Matter. **25**, 466002 (2013).
[32] T. Yamaguchi, J. Phys. Chem. Solids **35**, 479 (1974).